Photodissociation of triplet and singlet states of the CCO radical

Hyeon Choi, David H. Mordaunt, Ryan T. Bise, Travis R. Taylor, and Daniel M. Neumark
Department of Chemistry, University of California, Berkeley, California, 94720, and Chemical Sciences Division, Lawrence Berkeley National Laboratory, Berkeley, California 94720

(Received 24 October 1997; accepted 8 December 1997)

The triplet and singlet states of the ketenylidene (CCO) radical are investigated using fast radical beam photofragment translational spectroscopy, in which CCO is generated by laser photodetachment of CCO^- and subsequently photodissociated, and anion photoelectron spectroscopy. In the photodissociation experiment, two bands in which the upper state of CCO predissociates are studied. Photodissociation from excitation of the $\tilde{A}\,^3\Pi - \tilde{X}\,^3\Sigma^-$ band in CCO is observed from 16 666–23 529 cm^{-1}; resonances are observed and assigned to excited vibrational levels involving all three vibrational modes. We also report the first observation of the $\tilde{c}\,^1\Pi - \tilde{a}\,^1\Delta$ band in CCO. Here, the $\tilde{a}\,^1\Delta$ state of CCO is generated by laser photodetachment at higher photon energy than was used to generate the $\tilde{X}\,^3\Sigma$ state. The $\tilde{c}\,^1\Pi$ state is approximately located by photoelectron spectroscopy of CCO^-, and the photodissociation experiment shows that the origin of the $\tilde{c}\,^1\Pi - \tilde{a}\,^1\Delta$ band occurs around 17 170 cm^{-1}. Kinetic-energy release spectra from both bands yield accurate values for the C–CO bond dissociation energy and heat of formation of CCO: $D_0(\text{C–CO}) = 2.24 \pm 0.02$ eV (51.7 ± 0.5 kcal/mol) and $\Delta H^0_{f,298}(\text{CCO}) = 4.04 \pm 0.02$ eV (91.1 ± 0.5 kcal/mol). Although the translational-energy distributions resulting from excitation to the $\tilde{A}\,^3\Pi$ and $\tilde{c}\,^1\Pi$ states are clearly nonstatistical, consideration of the potential-energy surfaces indicates that dissociation from both states occurs via radiationless transitions to the $\tilde{X}\,^3\Sigma^-$ state. © *1998 American Institute of Physics.* [S0021-9606(98)03710-6]

I. INTRODUCTION

The ketenylidene (CCO) radical is an important reaction intermediate in interstellar cloud formation[1–3] and hydrocarbon combustion.[4–6] There is also growing interest in metal ketenylidene (CCO) complexes which can facilitate C–O, C–C, and C–H bond formation and cleavage in organometallic chemistry.[7] Two unresolved issues are addressed in this article. First, large uncertainties have existed in the heat of formation of CCO, hindering our understanding of these fundamental reaction mechanisms. Secondly, although many reactions are believed to proceed via singlet CCO species, a lack of spectroscopic information on the singlet states of CCO has prevented the identification of any singlet CCO radicals. In this paper, we address these two issues using a combination of photofragment translational spectroscopy and photoelectron spectroscopy.

The CCO radical was first identified spectroscopically by Jacox *et al.*[8] Its infrared spectrum was observed in a matrix isolation experiment and the CCO ground state was tentatively assigned to be a $^3\Sigma^-$ state. In addition, an unstructured absorption was seen near 500 nm which was attributed to CCO photodissociation, an interpretation supported by the depletion of the CCO absorption when the matrix was irradiated at that wavelength. The gas-phase absorption spectrum of CCO was subsequently recorded by Devillers and Ramsay.[9] They observed a rotationally resolved band with origin at 11 651 cm^{-1} and assigned it to the $\tilde{A}\,^3\Pi - \tilde{X}\,^3\Sigma^-$ transition, obtaining spectroscopic constants for both states. Laser induced fluorescence (LIF),[10] microwave,[11] and near IR (infrared) spectroscopy[12–16] were used to further establish the vibrational frequencies and spectroscopic constants for the $\tilde{X}\,^3\Sigma^-$ and the $\tilde{A}\,^3\Pi$ states.

The photoelectron spectrum of CCO^- was first taken by Oakes *et al.*[17] and the electron affinity of CCO was determined as 1.848 ± 0.003 eV. A more recent photoelectron spectrum by Zengin *et al.*[18] showed the electron affinity to be 2.29 ± 0.02 eV; the earlier value was attributed to vibrational hot bands.

CCO is known to have several low-lying singlet states in addition to the $\tilde{A}\,^3\Pi$ state. Walch[19] used polarization-configuration-interaction (POL-CI) with generalized valence bond (GVB) theory to characterize the triplet and singlet states. Chabalowski *et al.*[20] also performed calculations at the multireference double-excitation (MRCI) method. According to these studies, the molecular orbital configuration $\cdots(6\sigma)^2(1\pi)^4(7\sigma)^2(2\pi)^2$ leads to the $\tilde{X}\,^3\Sigma^-$, $\tilde{a}\,^1\Delta$, and $\tilde{b}\,^1\Sigma^+$ states, and the $\tilde{A}\,^3\Pi$ and $\tilde{c}\,^1\Pi$ states are derived from the $\cdots(6\sigma)^2(1\pi)^4(7\sigma)^1(2\pi)^3$ configuration. The energy ordering of the five electronic states is shown in Fig. 1. While the singlet states are not accessible by optical excitation from the $\tilde{X}\,^3\Sigma^-$ state, they are accessible by anion photodetachment; the molecular orbital configuration for the $\tilde{X}\,^2\Pi$ ground state of CCO^- is $(\cdots 6\sigma^2 1\pi^4 7\sigma^2 2\pi^3)$. Term values for the $\tilde{a}\,^1\Delta$ and $\tilde{b}\,^1\Sigma^+$ states were experimentally determined from the CCO^- photoelectron spectrum by Zengin *et al.*;[18] the higher lying $\tilde{c}\,^1\Pi$ state was apparently too high in energy to be seen at their highest photodetachment energy, 4.66 eV.

The heat of formation of CCO has been determined in several ways. The apparent photodissociation at 500 nm seen

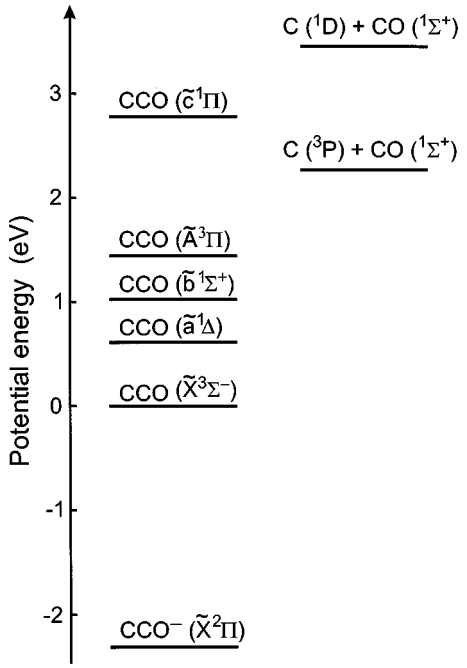

FIG. 1. Energetics of CCO electronic states.

by Jacox *et al.*[8] places a lower limit of 3.7 eV on its heat of formation. Becker and Bayes[4,5] observed CO chemiluminescence from the O+CCO reaction; based on this, along with the observation of Jacox, they deduced the CCO heat of formation to be 4.0 ± 0.2 eV. Both of these values are at variance with the 1985 ''literature value'' [21] of 2.9 ± 0.7 eV, obtained from the decomposition rate of C_3O_2.[22] However, the earlier values are in good agreement with recent values from *ab initio* calculation (3.86 eV)[19] and combined electron affinity and gas phase acidity measurements[18,23] (4.0 ± 0.2 eV). In this paper, we confirm and further refine the higher value for the CCO heat of formation.

Although experiment and theory have established the existence of low-lying singlet states in CCO, no optical transitions between these states have been observed. The absence of a spectroscopic probe for singlet CCO species has hindered verification of proposed reaction mechanisms in combustion, interstellar clouds, and photolysis of C_3O_2. For example, the ground states of C_3O_2 and CO molecules are $^1\Sigma^+$ states, so the formation of triplet CCO from the photolysis of C_3O_2[24–32] is spin-forbidden. Triplet CCO radicals are not observed under collisionless photolysis conditions, but are seen in the presence of collisions, presumably due to collisional quenching of singlet CCO.[10,27,29]

In this paper, we investigate the photodissociation spectroscopy and dynamics of triplet and singlet CCO using our fast radical beam photofragment translational spectrometer. In this experiment, CCO is generated by photodetachment of CCO^- and subsequently photodissociated. In all prior investigations of this type, care was taken to photodetach the ions at sufficiently low energy so that only ground-state radicals would be produced. This scheme is used to generate CCO $\tilde{X}\,^3\Sigma^-$ and we observe dissociation from upper state excited vibrational levels of the $\tilde{A}\,^3\Pi-\tilde{X}\,^3\Sigma^-$ band. In addition, we demonstrate that we can generate the CCO $\tilde{a}\,^1\Delta$ state by photodetachment at higher energy, and thus identify the $\tilde{c}\,^1\Pi-\tilde{a}\,^1\Delta$ transition for the first time. This work on the singlet state is aided considerably by photoelectron spectroscopy of CCO^- at a higher photon energy than that used by Zengin *et al.*,[18] enabling us to determine the approximate location of the $\tilde{c}\,^1\Pi$ state prior to performing the photodissociation experiments.

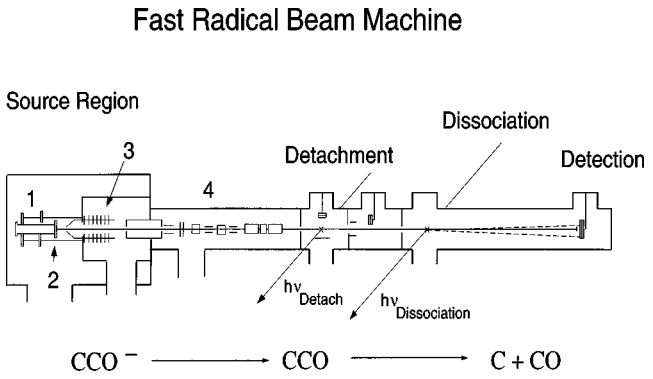

FIG. 2. Schematic of fast radical beam photofragment translational spectrometer. (1) Pulsed valve, (2) electric discharge, (3) acceleration plates, (4) Bakker-type time-of-flight mass spectrometer. Detachment, dissociation, and detection regions are also indicated.

II. EXPERIMENT

Two different instruments, a negative ion photoelectron spectrometer and a fast radical beam photofragment translational spectrometer, are used for this study. In both, the CCO^- anion is produced by electrical discharge of C_3O_2 molecules. C_3O_2 is synthesized by the dehydration of malonic acid with phosphorus pentoxide, as described by Brauer.[33] Ne gas (40 psi) flows over C_3O_2 which is kept in a glass bubbler cooled in a acetone/dry ice bath. The resultant mixture supersonically expands through a pulsed valve and electrical discharge[34] into the source region of the apparatus. A pulsed electrical discharge (-700 V) forms CCO^- anions; the discharge occurs in the beginning of supersonic expansion and the CCO^- anions are made and cooled to 20–50 K.

A detailed description of the photoelectron spectrometer is given elsewhere.[35,36] Briefly, negative ions generated in the ion source are injected into a time-of-flight mass spectrometer using a pulsed electric field. The ions separate in time and space according to their mass-to-charge ratio and are detected with a microchannel plate detector. The ion of interest is selectively photodetached using the fifth harmonic (5.822 eV) of a pulsed Nd:YAG laser. After detachment the kinetic energy of the electrons is determined by time-of-flight analysis, as described by Xu *et al.*[36] The instrumental resolution is 8 meV at 0.65 eV and degrades as $(\mathrm{eKE})^{3/2}$.

CCO photodissociation was studied using the fast radical beam photofragment spectrometer shown in Fig. 2. The experimental apparatus has been described in detail previously.[37,38] Negative ions formed in the source region are accelerated to 6 keV and separated temporally by a time-of-flight (TOF) mass spectrometer. The CCO^- ion packet is intersected by an excimer pumped pulsed dye laser beam,

photodetaching some anions to yield neutral CCO radicals. By changing the photodetachment energy, we can selectively detach CCO^- to make either ground $\tilde{X}\,^3\Sigma^-$ state only or ground $\tilde{X}\,^3\Sigma^-$ state plus $\tilde{a}\,^1\Delta$ state of CCO. Any remaining ions are removed by the application of an electrical deflection pulse. The neutral beam is then crossed by a second excimer-pumped tunable dye laser beam. Some neutrals absorb a photon and dissociate.

These photofragments are detected by microchannel plates. The high center-of-mass kinetic energy (6 keV) allows the fragment to be detected with high efficiency ($\sim 50\%$). The overall experiment is summarized as

$$CCO^- \xrightarrow{h\nu(\text{detach})} CCO \xrightarrow{h\nu(\text{dissociation})} C+CO. \quad (1)$$

Two types of experiment are performed. The photofragment yield (PFY) spectrum is obtained by collecting the total flux of fragments as a function of the photodissociation laser wavelength. We also probe the photodissociation dynamics by detecting both fragments in coincidence from a single parent CCO at a fixed photon energy for photodissociation. Using a time- and position-sensitive (TPS) wedge-and-strip anode detector[37] to measure the separation between the fragments and the interval between their arrival times, we obtain the kinetic-energy release and scattering angle for each dissociation event. From this the translational energy distribution $P(E_T)$ is determined. Because of the low translational energy release for this system, a very limited range of scattering angles is probed in this experiment, so angular distributions are not reported.

III. RESULTS

In this section, the experimental results are summarized, followed by *ab initio* calculations on the CCO radical. Specifically, the photoelectron spectrum of CCO^- at 5.822 eV is presented. The PFY spectra of CCO radicals are shown for the $\tilde{A}\,^3\Pi - \tilde{X}\,^3\Sigma^-$ and the $\tilde{c}\,^1\Pi - \tilde{a}\,^1\Delta$ bands. Finally, translational energy distributions $P(E_T)$ are presented for selected $\tilde{A}\,^3\Pi - \tilde{X}\,^3\Sigma^-$ and $\tilde{c}\,^1\Pi - \tilde{a}\,^1\Delta$ transitions.

A. Photoelectron spectrum of CCO^- anion

The photoelectron spectrum of CCO^- taken at 5.822 eV (213 nm) is shown in Fig. 3. The absolute peak positions and assignments are located in Table I. The spectrum consists of a series vibrationally resolved bands corresponding to transitions to several neutral electronic states. We observe all of the peaks reported by Zengin *et al.*[18] except for the $\tilde{a}\,^1\Delta$ (200) transition. In addition we see peaks labeled *K*, *L*, and *M* that were not observed previously. Peak *K* is assigned as the transition to the $\tilde{A}\,^3\Pi$ (003) state. Peaks *L* and *M* are too high in energy to correspond to a vibrational transition within the $\tilde{A}\,^3\Pi$ manifold, so we assign *L* and *M* to the origin and the (001) vibrational level of the $\tilde{c}\,^1\Pi$ state, respectively. Note that the $\tilde{A}\,^3\Pi$ and $\tilde{c}\,^1\Pi$ neutral states result from detachment of an electron from the 2π anion orbital and should therefore have the same photoelectron angular distribution. This is confirmed by photoelectron spectra taken at other laser polarization angles (not shown). From these assignments, the adiabatic electron affinity of CCO is

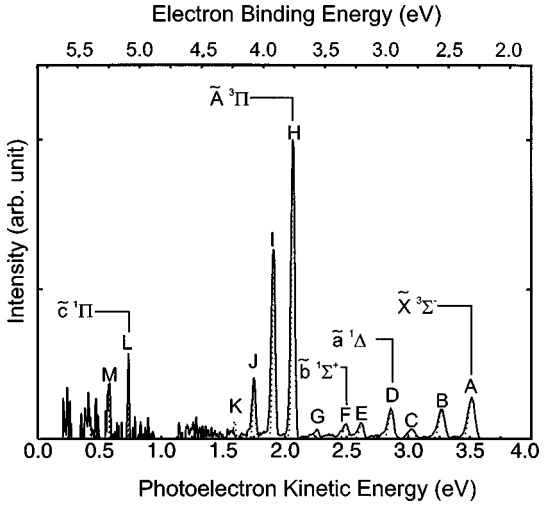

FIG. 3. Photoelectron spectrum of CCO at 5.822 eV taken at laser polarization $\theta = 0^0$.

2.310 ± 0.012 eV and the term values for the $\tilde{a}\,^1\Delta$ and $\tilde{c}\,^1\Pi$ states of CCO are 0.653 ± 0.017 eV and 2.775 ± 0.017 eV, respectively. The error bars on the electron affinity and $\tilde{a}\,^1\Delta$ term value are somewhat smaller than those reported by Zengin *et al.*[18]

B. Photofragment yield spectrum

With the aid of the photoelectron spectrum in Sec. III A, we can selectively form CCO in the ground $\tilde{X}\,^3\Sigma^-$ state, or in a combination $\tilde{X}\,^3\Sigma^-$ and $\tilde{a}\,^1\Delta$ states. To form neutral CCO in its ground $\tilde{X}\,^3\Sigma^-$ state with no vibrational excitation, we detach at 18 690 cm^{-1}, just above the photodetachment threshold (18 630 cm^{-1}). We can then measure the PFY spectrum from CCO $\tilde{X}\,^3\Sigma^-$ radicals.

To form neutral CCO in its $\tilde{a}\,^1\Delta$ electronic state with zero quanta of vibrational excitation, we detach at 24 210 cm^{-1}, just above the photodetachment threshold for this state (23 900 cm^{-1}). At this energy, one also produces CCO in its $\tilde{X}\,^3\Sigma^-$ state with the vibrational distribution shown in the photoelectron spectrum (Fig. 3). To identify

TABLE I. Peak position and assignments for the CCO^- photoelectron spectrum.

Peak	Assignment	Position (eV)	Splitting from origin (cm^{-1})[a]
A	$\tilde{X}\,^3\Sigma^-$ (000)	3.512	⋯
B	$\tilde{X}\,^3\Sigma^-$ (100)	3.269	1960
C	$\tilde{X}\,^3\Sigma^-$ (200)	3.019	3976
D	$\tilde{a}\,^1\Delta$ (000)	2.859	5267
E	$\tilde{a}\,^1\Delta$ (100)	2.618	7211
F	$\tilde{b}\,^1\Sigma^+$ (000)	2.488	8259
G	$\tilde{b}\,^1\Sigma^+$ (100)	2.262	10082
H	$\tilde{A}\,^3\Pi$ (000)	2.066	11663
I	$\tilde{A}\,^3\Pi$ (001)	1.909	12929
J	$\tilde{A}\,^3\Pi$ (002)	1.748	14228
K	$\tilde{A}\,^3\Pi$ (003)	1.577	15607
L	$\tilde{c}\,^1\Pi$ (000)	0.737	22382
M	$\tilde{c}\,^1\Pi$ (001)	0.584	23616

[a]All peak positions have an uncertainty of 12 meV.

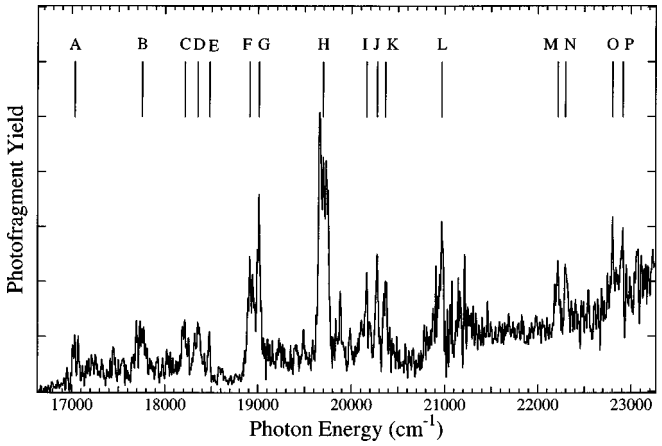

FIG. 4. Photofragment yield (PFY) spectrum of CCO for the $\tilde{A}\,^3\Pi - \tilde{X}\,^3\Sigma^-$ band. Assignments of labeled peaks are given in Table III.

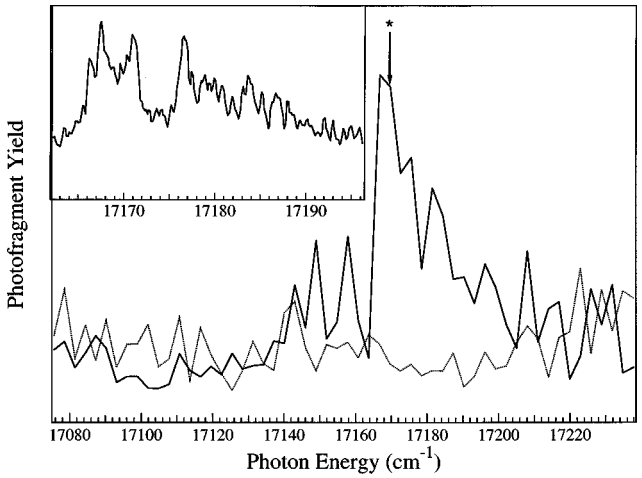

FIG. 5. Photofragment yield (PFY) spectrum of CCO for $\tilde{c}\,^1\Pi - \tilde{a}\,^1\Delta$ origin. Solid line: $\nu_{\text{Detach}} = 24\,210\ \text{cm}^{-1}$ (above the $\tilde{a}\,^1\Delta$ threshold). Dotted line: $\nu_{\text{Detach}} = 23\,070\ \text{cm}^{-1}$ (below the $\tilde{a}\,^1\Delta$ threshold. Inset shows finer scan (0.005 nm step) of the $\tilde{c}\,^1\Pi - \tilde{a}\,^1\Delta$ origin.

dissociation signal from the $\tilde{a}\,^1\Delta$ state, PFY spectra are repeated at a detachment energy $23\,070\ \text{cm}^{-1}$, just below the $\tilde{a}\,^1\Delta$ detachment threshold. The difference between PFY spectra obtained at 24 210 and $23\,070\ \text{cm}^{-1}$ is from CCO $\tilde{a}\,^1\Delta$ radicals.

The PFY spectrum obtained from CCO ($\tilde{X}\,^3\Sigma^-$) is shown Fig. 4. This spectrum covers $16\,660-23\,529\ \text{cm}^{-1}$ with $5.5-2.8\ \text{cm}^{-1}$ (0.1 nm) steps. Although the signal is weak, several sharp features are observed that are assigned to transitions to excited vibrational levels of the $\tilde{A}\,^3\Pi$ state (see Sec. IV A) that lie above the bond dissociation energy. The signal is weak because of poor Franck–Condon factors combined with low translational energy release (see Sec. IV B); the latter effect reduces our photofragment collection efficiency. Note that no dissociation is observed until well above the $\tilde{A}\,^3\Pi - \tilde{X}\,^3\Sigma^-$ origin at $11\,651\ \text{cm}^{-1}$,[9] because the lower vibrational levels are bound. Also, we do observe dissociation around 500 nm, a result consistent with the interpretation of the matrix experiments put forth by Jacox *et al.*[8]

The PFY spectrum obtained from CCO ($\tilde{a}\,^1\Delta$) is shown Fig. 5. Based on the photoelectron spectrum in Fig. 3, the origin of the $\tilde{c}\,^1\Pi - \tilde{a}\,^1\Delta$ band should occur at $17\,115 \pm 140\ \text{cm}^{-1}$. The main part of Fig. 5 shows spectra taken from $17\,080-17{,}220\ \text{cm}^{-1}$ at 0.1 nm($\sim 3\ \text{cm}^{-1}$) resolution. The dotted line shows data using $\nu_{\text{detach}} = 23\,070\ \text{cm}^{-1}$ and the solid line shows data using $\nu_{\text{detach}} = 24\,210\ \text{cm}^{-1}$. The large peak seen at $17\,170\ \text{cm}^{-1}$ in the spectrum taken at the higher detachment energy is assigned to the $\tilde{c}\,^1\Pi - \tilde{a}\,^1\Delta$ origin. The inset in Fig. 5 shows a finer scan with 0.005 nm ($\sim 0.15\ \text{cm}^{-1}$) steps and shows partially resolved rotational structure. No further structure is resolved using an etalon, with which the resolution of the laser is $0.04\ \text{cm}^{-1}$. Based on our term value for the $\tilde{a}\,^1\Delta$ state, 0.653 ± 0.017 eV, the term value for the $\tilde{c}\,^1\Pi$ state is 2.782 ± 0.017 eV.

C. Translational energy distribution of photofragments

Translational energy distributions $P(E_T)$ were obtained at selected peaks in the $\tilde{A}\,^3\Pi - \tilde{X}\,^3\Sigma^-$ and $\tilde{c}\,^1\Pi - \tilde{a}\,^1\Delta$ absorption bands. Figure 6 shows the $P(E_T)$ distribution obtained at $19\,660\ \text{cm}^{-1}$ (2.44 eV), the strongest peak in the $\tilde{A}\,^3\Pi - \tilde{X}\,^3\Sigma^-$ band. The distribution is binned in steps of 10 meV. The photofragment mass spectrum in the inset of Fig. 6 shows peaks at mass 12 and 28, corresponding to C+CO. The $P(E_T)$ distribution consists of a sharp peak centered around 0.15 eV with an abrupt drop in intensity toward higher translational energy. The maximum kinetic energy at which signal is seen is 0.20 ± 0.02 eV.

Figure 7 shows the $P(E_T)$ distribution obtained from excitation of the $\tilde{c}\,^1\Pi - \tilde{a}\,^1\Delta$ band at $17\,170\ \text{cm}^{-1}$, marked with an * in Fig. 5. The same photofragment mass spectrum is seen as in Fig. 6. This $P(E_T)$ distribution consists of two peaks centered at 0.5 and 0.23 eV, corresponding to C+CO ($v = 0,1$). The higher energy peak drops off abruptly at a maximum kinetic energy of 0.54 ± 0.02 eV.

D. *Ab initio* calculations

Ab initio calculations were performed to better understand how the various electronic states of CCO are coupled

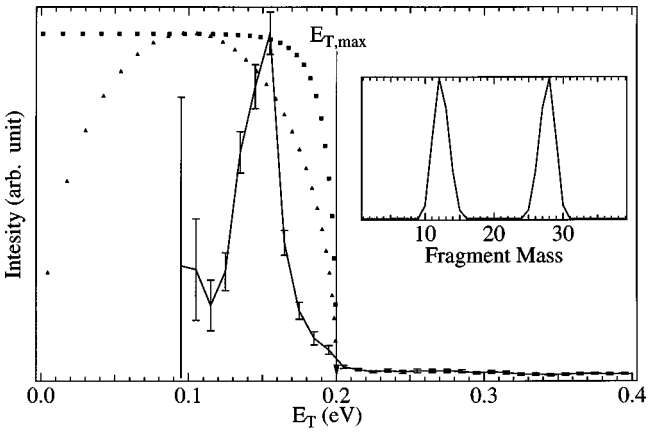

FIG. 6. Translational energy distribution $P(E_T)$ of C+CO products from excitation of $1_0^4\ \tilde{A}\,^3\Pi - \tilde{X}\,^3\Sigma$ transition ($h\nu_{\text{dissociate}} = 2.44$ eV). Inset shows the photofragment mass spectrum of CCO. Solid line: Experimental data. The $P(E_T)$ dist ibutions calculated from the prior distribution and phase space theory are shown as ▲ and ■, respectively.

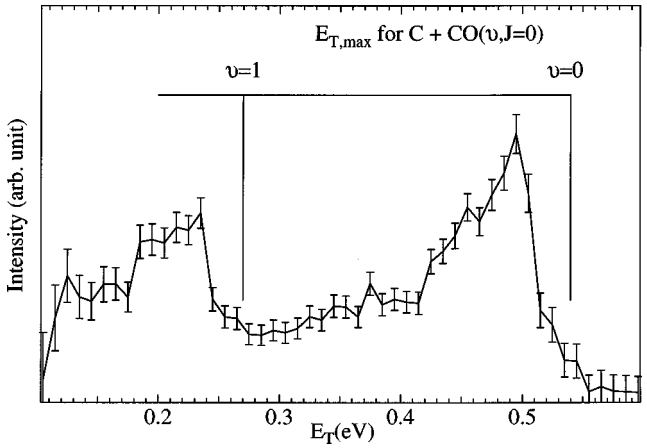

FIG. 7. Translational energy distribution $P(E_T)$ of CCO at the $\tilde{c}\,^1\Pi - \tilde{a}\,^1\Delta$ origin transition ($h\nu_{\mathrm{Diss}} = 2.13$ eV).

to the dissociation continuum. The lowest energy dissociation channel, $C(^3P) + CO(^1\Sigma^+)$, correlates with the $\tilde{X}\,^3\Sigma^-$ state and *a* $^3\Pi$ state. The molecular orbital configuration for this $^3\Pi$ state (hereafter referred to as the $\tilde{U}\,^3\Pi$ state) is $\cdots(6\sigma)^2(1\pi)^4(7\sigma)^2(2\pi)^1(8\sigma)^1$. This is therefore not the $\tilde{A}\,^3\Pi$ state, for which the molecular orbital configuration is $\cdots(6\sigma)^2(1\pi)^4(7\sigma)^1(2\pi)^3$; the $\tilde{A}\,^3\Pi$ state asymptotically correlates with excited state triplet products, $C(^3P) + CO(^3\Pi)$. The 8σ orbital is C–C antibonding, suggesting that the $\tilde{U}\,^3\Pi$ state is repulsive. These qualitative considerations imply that a diabatic crossing occurs between the $\tilde{A}\,^3\Pi$ state and a repulsive $^3\Pi$ state, as shown in Fig. 8. The object of our *ab initio* calculations was to determine the effect of this crossing on the dissociation dynamics.

Calculations were performed using the CASSCF(8,8) method with a 6-31 G* basis within the GAUSSIAN 92 suite of programs.[39] The active space consists of six Π orbitals (1Π, 2Π, 3Π) and two σ orbitals (7σ, 8σ). R_{CO} is optimized at

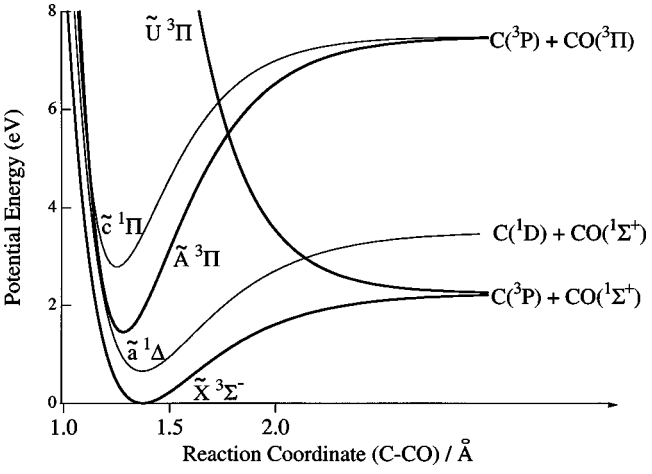

FIG. 8. Schematic potential-energy curves for the ground and excited states of CCO radical, illustrating correlations with the ground and excited state C+CO products. The energy spacings from the ground state to excited states of CCO and the C–CO bond dissociation energy are determined by our present work. Minimum energy configurations are obtained from Ref. 18 and the crossing point between the $\tilde{A}\,^3\Pi$ and the $\tilde{U}\,^3\Pi$ is obtained from the *ab initio* calculation described in the text.

TABLE II. Fitting parameters for calculating position of absorption ($\tilde{A}\,^3\Pi - \tilde{X}\,^3\Sigma^-$ of CCO). (Unit: cm^{-1})

	$\tilde{A}\,^3\Pi$ (cm^{-1})	
T_0	11,651.2 (Ref. 12)	
ω_1	2068.6 (Ref. 9)	
$\omega_1\chi_1$	11.45	
ω_2	601.25 (Refs. 15 and 16)	
$\omega_2\chi_2$	3.25	
ω_3	1284 (Ref. 16)	
$\omega_3\chi_3$	0.0	
	$n_2=2$	$n_2=1$
A_{SO}	−35.614 (Ref. 16)	−35.1667 (Ref. 15)
$\epsilon\omega_2$	104 (Ref. 16)	104.5 (Ref. 15)

each R_{CC} and the linear configuration is determined to be the minimum energy configuration for all values of R_{CC}. The calculation predicts the crossing between the $\tilde{A}\,^3\Pi$ state and a repulsive $^3\Pi$ state to occur at $R_{CC} = 1.774$ Å and $R_{CO} = 1.142$ Å, which is 5.5 eV above the $\tilde{X}\,^3\Sigma^-$ minimum for which $R_{CC} = 1.388$ Å and $R_{CO} = 1.149$ Å.

At this level of calculation, the term value for the $\tilde{A}\,^3\Pi$ state is 1.617 eV, while the experimental value is 1.445 eV.[12] Also, the calculated sum of R_{CC} and R_{CO} is 2.54 Å for the $\tilde{X}\,^3\Sigma^-$ state and 2.45 Å for the $\tilde{A}\,^3\Pi$ state, both of which lie close to the experimental values of 2.52 and 2.45 Å, respectively.[9]

The diabatic crossing occurs well above the onset of dissociation in the PFY spectrum ($\sim$2.4 eV). The energy of this crossing may be too high because of the limited accuracy of the calculation. Moreover, the two adiabatic curves repel each other in the crossing region, so that the effective barrier to dissociation of the $\tilde{A}\,^3\Pi$ along the lower adiabatic will be somewhat less than the energy of the diabatic crossing point. Nonetheless, the calculations certainly suggest that dissociation of the $\tilde{A}\,^3\Pi$ in the energy range probed by our experiment does not occur by coupling to the repulsive $\tilde{U}\,^3\Pi$ state. The dissociation mechanism is discussed further in Sec. V.

IV. ANALYSIS

In this section, we analyze the resonances in the photofragment yield spectrum for the $\tilde{A}\,^3\Pi - \tilde{X}\,^3\Sigma^-$ band of CCO and discuss the energetics of CCO radical dissociation.

A. Photofragment yield spectrum

Previous LIF and absorption studies of the CCO $\tilde{A}\,^3\Pi - \tilde{X}\,^3\Sigma^-$ transition[9,10,12,15,16] have yielded an accurate set of spectroscopic constants for the lower vibrational levels of the $\tilde{A}\,^3\Pi$ state, including vibrational frequencies for the ν_1 (C–O stretch), ν_2 (CCO bend), and ν_3 (C–C stretch) modes, anharmonicities for the ν_1 and ν_2 modes, rotational constants, spin–orbit coupling and Renner–Teller parameters. These are listed in Table II. The energy level pattern due to Renner–Teller coupling in a $^3\Pi$ electronic state is given by Hougen.[40] We can use these constants to predict the location of the higher-lying vibrational levels, and thus as-

TABLE III. Peak assignment (cm^{-1}) for PFY spectrum of CCO. Calculated positions are obtained based on parameters in Table II.

	Experimental peak position (cm^{-1})	Calculated position (cm^{-1})	Assignment/$E(n_2K,P)$[a]
A	17 035	17 046	$1_0^2 2_0^2/E^+(2,1,0)$
B	17 756	17 720	1_0^3
C	18 216	18 288	$1_0^2 3_0^2$
D	18 353	18 330	$1_0^2 2_0^2 3_0^1/E^+(2,10)$
E	18 479	18 414	$1_0^3 2_0^1/E^+(1,0,0)$
F	18 911	18 982	$1_0^2 2_0^1 3_0^2/E^+(1,0,0)$
G	19 012	19 004	$1_0^3 3_0^1$
		19 046	$1_0^3 2_0^2/E^+(2,1,0)$
H	19 698	19 697	1_0^4
I	20 166	20 288	$1_0^3 3_0^2$
J	20 277	20 330	$1_0^3 2_0^2 3_0^1/E^+(2,1,0)$
K	20 367	20 391	$1_0^4 2_0^1/E^+(1,0,0)$
L	20 970	20 981	$1_0^4 3_0^1$
		21 023	$1_0^4 2_0^2/E^+(2,1,0)$
M	22 219	22 265	$1_0^4 3_0^2$
N	22 298	22 307	$1_0^4 2_0^2 3_0^1/E^+(2,1,0)$

[a]Energies $E(n_2,K,P)$ of various vibronic states are characterized by a set of quantum numbers, n_2, K(the resultant vibronic angular momentum $=|\pm\Lambda\pm l|$), and P(the resultant vibronic angular momentum including spin$=|\pm\Omega\pm l|$). The upper Renner–Teller state is expressed by E^+, and the lower by E^-, which is not observed in our present work.

sign most of the features seen in the PFY spectrum in Fig. 4. The predicted energies and assignments of the PFY resonances are listed in Table III.

Peak *H*, the most prominent peak, centered at 19 698 cm^{-1}, is assigned to the 1_0^4 transition. This peak is actually a triplet split by 35 cm^{-1} corresponding to the three spin–orbit components of the $\tilde{A}\,^3\Pi$ state. This splitting agrees well with that seen for several of the lower-lying levels.[9,12,15,16] Transitions involving the other two modes also contribute to the PFY spectrum. Although this is a linear-to-linear transition, the bending mode is active due to the large difference of bending frequency in the $\tilde{X}$ (379.53 cm^{-1})[14] and $\tilde{A}$ (594.75 cm^{-1})[15] states and strong Renner–Teller coupling in the $\tilde{A}$ state.[15,16] Some of the assignments are ambiguous, especially those involving the bending mode. These problems arise in part because of a 2:1 Fermi resonance between the ν_2 and ν_3 modes (see Table II) as noted in previous studies.[9,10,16] Nonetheless the agreement between the experimental and predicted energies is generally reasonable, supporting the assignments in Table III.

B. Translational energy distributions

1. CCO thermochemistry

The $P(E_T)$ distributions in Figs. 6 and 7 yield information on the CCO dissociation energy and the partitioning of excess energy among the product degrees of freedom. Energy conservation dictates that

$$h\nu_{\rm diss}+E_{\rm INT}({\rm CCO})=D_0({\rm C–CO})+E_{\rm INT}({\rm C+CO})+E_T({\rm C+CO}), \quad (2)$$

where $E_{\rm INT}$(CCO) is the initial energy of the CCO, $E_{\rm INT}$(C+CO) is the product internal energy, and E_T(C+CO) is the product translational energy. At the maximum allowed kinetic energy, $E_{T\max}$, $E_{\rm INT}$(C+CO)$=0$. The bond dissociation energy can therefore be determined from the $P(E_T)$ distribution provided that the value of $E_{T\max}$ is clear.

The $P(E_T)$ spectrum for the $\tilde{A}\,^3\Pi–\tilde{X}\,^3\Sigma^-$ transition shown in Fig. 6 is obtained at $h\nu_{\rm diss}=19\,660\ cm^{-1}$ (2.44 eV). The spectrum drops off abruptly on the high energy side of the peak maximum at 0.15 eV; no signal is seen beyond $E_T=0.20\pm0.02$ eV, and this is taken to be $E_{T\max}$. Although no rotational structure is resolved in the PFY spectrum of CCO, we estimate a rotational temperature of 35 K from our previous study of HCCO photodissociation,[41] so $\langle E_{\rm INT}({\rm CCO})\rangle\approx0.002$ eV. Thus the bond dissociation energy for C–CO is determined: D_0(C–CO)$=2.24\pm0.02$ eV (51.7 ±0.5 kcal/mol) at 0 K.

The $P(E_T)$ distribution in Fig. 7 is obtained from excitation of the $\tilde{c}\,^1\Pi–\tilde{a}\,^1\Delta$ vibrational band origin at $h\nu_{\rm diss}=2.128$ eV (17 170 cm^{-1}). The abrupt drop-off in the higher energy peak yields $E_{T\max}=0.54\pm0.02$ eV. For this band, $E_{\rm INT}$(CCO) includes the term energy for the $\tilde{a}\,^1\Delta$ state, 0.653 ± 0.017 eV. We then obtain a bond dissociation energy for C–CO, D_0(C–CO)$=2.24\pm0.03$ eV (51.7 ±0.7 kcal/mol) at 0 K. This value is in excellent agreement with that obtained from Fig. 6, supporting our selection of $E_{T\max}$ in both cases. The uncertainty in D_0(C–CO) is slightly higher when derived from the data in Fig. 7 because of the uncertainty in the electronic term value of the $\tilde{a}\,^1\Delta$ state.

Based on our value of D(C–CO), no dissociation signal should be observed at excitation energies below 18 065 cm^{-1}. However, peaks *A* and *B* in the PFY spectrum, Fig. 4, lie below this energy. While these could be hot band transitions, Table III shows that they can be assigned to transitions originating from the (000) level of the $\tilde{X}\,^3\Sigma^-$ state. It is possible that they arise from resonant two-photon excitation via the intermediate $\tilde{A}\,^3\Pi$ levels listed in Table III. Unfortunately the dissociation signal at these energies was too low to permit measurement of the translational energy distributions.

The heat of formation of CCO is determined from the bond dissociation energy and heats of formation of C[$\Delta H_{f,0}^0$(C)$=7.371\pm0.005$ eV] and CO[$\Delta H_{f,0}^0$(CO) $=-1.180\pm0.002$ eV].[21] This yields $\Delta H_{f,0}^0$(CCO)$=3.95$ ±0.02 eV (91.1$\pm$0.5 kcal/mol). These values can be scaled to values at standard temperature (298.15 K). Using known vibrational frequencies of the CCO $\tilde{X}\,^3\Sigma^-$ state,[10,13,14] we obtain $\Delta H_{f,298}^0$(CCO)$=4.04\pm0.02$ eV. This value agrees with the recent determination from the CCO photoelectron spectrum, $\Delta H_{f,298}^0$(CCO)$=3.99\pm0.20$ eV,[18] but our error bars are considerably lower.

The heat of formation of CCO^- can be determined from this heat of formation, the electron affinity of CCO and the integrated heat capacity of electron: $\Delta H_{f,298}^0$(CCO)$=1.67$ ±0.02 eV. The gas-phase acidity of HCCO can be also calculated from the heats of formation of H^+,[42] CCO^-, and HCCO,[41] as follows.

$$\Delta H^0_{\text{acid},298}(\text{HCCO}) = \Delta H^0_{f,298}(H^+) + \Delta H^0_{f,298}(\text{CCO}^-) - \Delta H^0_{f,298}(\text{HCCO}) = 15.76 \pm 0.04 \text{ eV}. \quad (3)$$

The enthalpy for acid association of HCCO was determined by Van Doren *et al.*: $15.45(\pm 0.12)$ eV $< \Delta H^0_{\text{acid},298\text{ K}}(\text{HCCO}) < 15.87(\pm 0.12)$ eV.[23] This is in good agreement with our value.

2. Product energy distributions

From the bond dissociation energy determined above, the single peak seen in the $P(E_T)$ spectrum in Fig. 6 corresponds entirely to $C+CO(v=0)$; $C+CO(v=1)$ products are not energetically accessible. The width of the peak in this spectrum therefore indicates the extent of rotational excitation in the CO fragment. We find that $f_R = 0.25$, where f_R is the fraction of available energy appearing as product rotation. In Fig. 7, however, $E_{\text{INT}}(\text{CCO})$ is sufficiently large so that the $C+CO(v=1)$ state is energetically accessible. This is the origin of the lower energy peak centered at 0.23 eV. Roughly 40% of the CO product is in the $v=1$ state. We also observe broad features to the low energy side of each peak, which correspond to the rotational excitation of CO product. The overall partitioning of available energy among product translation, vibration, and rotation is $f_T = 0.6$, $f_v = 0.2$, and $f_R = 0.2$, respectively.

It is useful to compare the experimental distributions with those obtained from simple statistical models. Shown in Fig. 6 along with the experimental data are the translational energy distributions expected for a prior distribution (▲)[43] and from phase space theory (PST) (■).[44–46] The prior and PST distributions are calculated using Eqs. (4) and (5), respectively

$$P(E_T) = \sum_{J_{\text{CO}}} (2J_{\text{CO}}+1)(E_T)^{1/2} \cdot \delta(h\nu - D_0 - E_t - B \cdot J_{\text{CO}}(J_{\text{CO}}+1)), \quad (4)$$

$$P(E_T) = \sum_{J_{\text{CCO}}} \sum_{J_{\text{CO}}} P_{\text{Bolt}}(J_{\text{CCO}}) \cdot (2J'+1) \cdot \delta(h\nu - D_0 - E_T - B \cdot J_{\text{CO}}(J_{\text{CO}}+1)), \quad (5)$$

where J_{CO} and J_{CCO} are the angular momenta of CO and CCO, B is the rotational constant of CO fragment, and $P_{\text{Bolt}}(J_{\text{CCO}})$ is the Boltzmann distribution assuming $T_{\text{rot}} = 35$ K. In Eq. (5), $J' = J_{\text{CCO}}$ when $J_{\text{CO}} \geqslant J_{\text{CCO}}$ and $J' = J_{\text{CO}}$ when $J_{\text{CO}} < J_{\text{CCO}}$. Both statistical models predict a considerably broader rotational distribution with more rotational excitation of the CO than is observed experimentally.

We have also calculated the prior distribution expected for the singlet–singlet transition in Fig. 7. This predicts 26% of the CO product to be in $v=1$, with the overall energy partitioning given by $f_T = 0.52$, $f_v = 0.13$, and $f_R = 0.35$. The experimental distribution shows more CO vibrational excitation and less rotational excitation. It therefore appears that neither of the experimental $P(E_T)$ distributions can be reproduced by statistical models. This is discussed further in the next section.

V. DISCUSSION

In this section we consider the dissociation mechanism subsequent to excitation of the $\widetilde{A}\ ^3\Pi$ and $\widetilde{c}\ ^1\Pi$ states. The PFY spectra in Figs. 4 and 5 are structured, indicating that excitation in each case is to a bound state that undergoes predissociation. As discussed in Sec. III D and displayed in Fig. 8, the $\widetilde{A}\ ^3\Pi$ state correlates diabatically to excited $C(^3P)+CO(^3\Pi)$ products that lie well above the excitation energies in this study. In order to undergo dissociation to $C(^3P)+CO(^1\Sigma^+)$ products, the $\widetilde{A}\ ^3\Pi$ state must decay either by coupling to the repulsive $\widetilde{U}\ ^3\Pi$ state, or by internal conversion to the ground $\widetilde{X}\ ^3\Sigma^-$ state.

The PFY spectrum and $P(E_T)$ distribution in Fig. 6 shows that the onset for dissociation from the $\widetilde{A}\ ^3\Pi$ state occurs at or just above the C–CO bond dissociation energy. Given the high energy of the crossing point between the $\widetilde{U}\ ^3\Pi$ and $\widetilde{A}\ ^3\Pi$ states, it is unlikely that predissociation via the repulsive $\widetilde{U}\ ^3\Pi$ state would occur so close to the thermodynamic threshold for dissociation. On the other hand, if there were no barrier along the reaction coordinate for dissociation of the $\widetilde{X}\ ^3\Sigma^-$ state, internal conversion to this state would lead to dissociation as soon as the bond dissociation energy is exceeded. This therefore appears to be the dissociation mechanism for the $\widetilde{A}\ ^3\Pi$ state.

In Fig. 6, both statistical distributions result in considerably more CO rotational excitation than is seen experimentally, indicating that dissociation on the ground state following internal conversion is nonstatistical in nature. This is qualitatively consistent with the relatively shallow well and small number of vibrational modes, both of which might be expected to lead to very rapid dissociation. More quantitatively, one does not expect statistical dissociation unless the RRKM (Rice–Ramsperger–Kassel–Marcus) dissociation rate is considerably less than the characteristic vibrational frequencies; this condition allows intra-vibrational relaxation (IVR) to occur prior to dissociation.[47]

The RRKM dissociation rate is given by

$$k_{\text{RRKM}}(E) = \frac{G(E-D_0)}{hN(E)}, \quad (6)$$

where $G(E-D_0)$ is the sum of states for the active degrees of freedom in the transition state and $N(E)$ is the reactant density of states. The ground state of CCO ($\widetilde{X}\ ^3\Sigma^-$ state) can correlate with the lowest dissociation channel $[C(^3P)+CO(^1\Sigma^+)]$ without orbital change, so no barrier on $\widetilde{X}\ ^3\Sigma^-$ state of CCO is expected. We thus take the transition state to correspond to C+CO products. The RRKM dissociation rate is then calculated by using the four vibrational degrees of freedom of CCO ($\widetilde{X}\ ^3\Sigma^-$ state) for the reactant and the two rotational and one vibrational degrees of freedom of CO fragment for the transition state. We find $k_{\text{RRKM}}(E) = 5.04 * 10^{12}\ \text{s}^{-1}$, which is higher than the bend frequency on the ground state, $2.51 * 10^{12}\ \text{s}^{-1}$. Under these circumstances it is not surprising that a nonstatistical product energy distribution is observed.

We next consider dissociation of the $\widetilde{c}\ ^1\Pi$ state. Only the $C(^3P)+CO(^1\Sigma^+)$ channel is energetically accessible, so

intersystem crossing to a triplet state must occur prior to dissociation. As was the case with the $\tilde{A}\,^3\Pi$ state, the crossing point with the $\tilde{U}\,^3\Pi$ state is most likely too high in energy for dissociation by this state to be a viable mechanism, and it is more reasonable to expect dissociation to occur by intersystem crossing to the $\tilde{X}\,^3\Sigma^-$ state. This may occur directly, or through one or both of the electronic states that lie between the $\tilde{c}\,^1\Pi$ and $\tilde{X}\,^3\Sigma^-$ states. Since the internal energy on the ground state resulting from this process is considerably higher than for the $\tilde{A}\,^3\Pi$ state level responsible for the translational energy distribution in Fig. 6, one again expects a nonstatistical product energy distribution. This is consistent with the experimental distribution in Fig. 7,which, as discussed in Sec. IV B 2, has considerably less energy in CO rotation and more energy in CO vibration than would be expected from a statistical model.

We have previously found that the dissociation yield from the vibrationless level of an excited electronic state is less than unity even if this level is well above the dissociation threshold.[41,48] This suggests that it may be possible to observe the vibrational origin of the $\tilde{c}\,^1\Pi-\tilde{a}\,^1\Delta$ band by laser-induced fluorescence. Such an observation would be extremely useful as a probe of singlet CCO.

VI. CONCLUSIONS

This paper reports the first study of the photodissociation spectroscopy and dynamics of the CCO radical. Photofragment yield (PFY) spectra and photofragment translational energy distributions are obtained using our fast radical beam photofragment translation spectroscopy instrument. We observe predissociation from excited vibrational levels of the $\tilde{A}\,^3\Pi$ state that are accessed by excitation of the $\tilde{A}\,^3\Pi-\tilde{X}\,^3\Sigma^-$ band, and from the ground vibrational level of the $\tilde{c}\,^1\Pi$ state via excitation of the $\tilde{c}\,^1\Pi-\tilde{a}\,^1\Delta$ band. In both cases, the lower state of CCO is generated by laser photodetachment of CCO. The $\tilde{X}\,^3\Sigma^-$ state is formed using a detachment energy just above the electron affinity of CCO, while the $\tilde{a}\,^1\Delta$ state is formed at a detachment energy sufficiently high to access this low-lying excited state of CCO. The location of the $\tilde{c}\,^1\Pi$ was unknown prior to this work. We located it approximately by photoelectron spectroscopy of CCO at a photodetachment energy of 5.82 eV, obtaining a term value of 2.775 ± 0.020 eV for the $\tilde{c}\,^1\Pi$ state. This enabled us to find the $\tilde{c}\,^1\Pi-\tilde{a}\,^1\Delta$ band origin at 17 170 cm^{-1} (2.128 eV) using photodissociation spectroscopy.

The PFY spectrum for the $\tilde{A}\,^3\Pi-\tilde{X}\,^3\Sigma^-$ band consists of a series of transitions to vibrationally excited levels of the $\tilde{A}\,^3\Pi$ state that lie above the dissociation threshold. These transitions, reported here for the first time, can be assigned based on spectroscopic constants from earlier absorption and laser-induced fluorescence studies of CCO. Our observation of the $\tilde{c}\,^1\Pi-\tilde{a}\,^1\Delta$ band origin represents the first observation of a transition between singlet states of CCO, and may be useful as a diagnostic for singlet CCO in combustion and other applications.

Product translational energy distributions from excitation of the triplet and singlet bands yield the CCO bond dissociation energy and the partitioning of available energy among the product degrees of freedom. The bond dissociation energy is 2.24 ± 0.02 eV, yielding $\Delta H^0_{f,298}(\mathrm{CCO})=4.04\pm0.02$ eV. The translational energy distribution for the 1^4_0 transition of the triplet band shows that all the CO is in its $v=0$ level (the only energetically accessible level), while a mixture of CO $v=0$ and $v=1$ level results from the origin transition of the $\tilde{c}\,^1\Pi-\tilde{a}\,^1\Delta$ band. In both cases, the distributions are highly nonstatistical. Nonetheless, comparison with *ab initio* calculations implies that the $\tilde{A}\,^3\Pi$ and $\tilde{c}\,^1\Pi$ states dissociate via internal conversion and intersystem crossing, respectively, to the ground $\tilde{X}\,^3\Sigma^-$ state.

ACKNOWLEDGMENTS

This research is supported by the Director, Office of Energy Research, Office of Basic Energy Sciences, Chemical Sciences Division, of the U.S. Department of Energy under Contract No. DE-AC03-76SF00098. We thank Professor Robert E. Continetti for sharing his results prior to publication. D.M.N. is a Canulle and Henry Dreyfus Teacher-Scholar.

[1] R. D. Brown, D. M. Cragg, P. D. Godfrey, W. M. Irvine, D. McGonagle, and M. Ohishi, Origins Life Evol. Biosphere **21**, 399 (1992).
[2] W. M. Irvine, Adv. Space Res. **15**, 35 (1995).
[3] M. Ohishi, H. Suzuki, S. I. Ishikawa, C. Yamada, H. Kanamori, W. M. Irvine, R. D. Brown, P. D. Godfrey, and N. Kaifu, Astrophys. J. **380**, L39 (1991).
[4] K. H. Becker and K. D. Bayes, J. Chem. Phys. **48**, 653 (1968).
[5] K. D. Bayes, J. Chem. Phys. **52**, 1093 (1970).
[6] A. Fontijn and S. E. Johnson, J. Chem. Phys. **59**, 6193 (1973).
[7] G. Geoffroy and S. L. Bassner, Adv. Organomet. Chem. **28**, 1 (1988).
[8] M. E. Jacox, D. E. Milligan, N. G. Moll, and W. E. Thompson, J. Chem. Phys. **43**, 3734 (1965).
[9] C. Devillers and D. A. Ramsay, Can. J. Phys. **49**, 2839 (1971).
[10] W. M. Pitts, V. M. Donnelley, A. P. Baronavski, and J. R. McDonald, Chem. Phys. **61**, 451 (1981).
[11] Y. Ohshima, Y. Endo, and T. Ogata, J. Chem. Phys. **102**, 1493 (1995).
[12] M. Fujitake, R. Kiryu, and N. Ohashi, J. Mol. Spectrosc. **154**, 169 (1992).
[13] C. Yamada, H. Kanamori, H. Horiguchi, S. Tsuchiya, and E. Hirota, J. Chem. Phys. **84**, 2573 (1986).
[14] N. Ohashi, R. Kiryu, S. Okino, and M. Fujitake, J. Mol. Spectrosc. **157**, 50 (1993).
[15] H. Abe, T. Kikuchi, K. Takahashi, M. Fujitake, and N. Ohashi, J. Mol. Spectrosc. **167**, 353 (1994).
[16] H. Abe, Y. Kawamoto, M. Fujitake, N. Ohashi, T. Momose, and T. Shida, J. Mol. Spectrosc. **180**, 277 (1996).
[17] J. M. Oakes, M. E. Jones, V. M. Bieberbaum, and G. B. Ellison, J. Phys. Chem. **87**, 4810 (1983).
[18] V. Zengin, B. J. Persson, K. M. Strong, and R. E. Continetti, J. Chem. Phys. **105**, 9740 (1996).
[19] S. P. Walch, J. Chem. Phys. **72**, 5679 (1980).
[20] C. F. Chabalowski, R. J. Buenker, and S. D. Peyerimhoff, J. Chem. Phys. **84**, 268 (1986).
[21] JANAF Thermochemical Tables, J. Phys. Chem. Ref. Data **14**, Supplement No. 1 (1985).
[22] H. B. Palmer and W. D. Cross, Carbon **3**, 475 (1966).
[23] J. M. Van Doren, T. M. Miller, A. E. S. Miller, A. A. Viggiano, R. A. Morris, and J. F. Paulson, J. Am. Chem. Soc. **115**, 7407 (1993).
[24] D. G. Williamson and K. D. Bayes, J. Am. Chem. Soc. **90**, 1957 (1968).
[25] K. D. Bayes, J. Am. Chem. Soc. **84**, 4077 (1962).
[26] K. D. Bayes, J. Am. Chem. Soc. **85**, 1730 (1963).
[27] T. Morrow and W. D. McGrath, Trans. Faraday Soc. **62**, 3142 (1966).
[28] W. Bauer, R. Meuser, and K. H. Becker, J. Photochemistry **24**, 99 (1984).
[29] K. H. Becker, R. Konig, R. Meuser, P. Wiesen, and K. D. Bayes, J. Photochem. Photobiol., A: Chem. **64**, 1 (1992).
[30] J. McFarlane, J. C. Polanyi, J. G. Shapter, and J. M. Williamson, J. Photochem. Photobiol., A: Chem. **46**, 139 (1989).
[31] D. J. Anderson and R. N. Rosenfeld, J. Chem. Phys. **94**, 7857 (1991).

[32] C. E. M. Strauss, S. H. Kable, G. K. Chawla, P. L. Houston, and I. R. Burak, J. Chem. Phys. **94**, 1837 (1991).
[33] G. Brauer, *Handbook of Preparative Inorganic Chemistry*, 2nd ed. (Academic, New York, 1963).
[34] D. L. Osborn, D. J. Leahy, D. R. Cyr, and D. M. Neumark, J. Chem. Phys. **104**, 5026 (1996).
[35] R. B. Metz, A. Weaver, S. E. Bradforth, T. N. Kitsopoulos, and D. M. Neumark, J. Phys. Chem. **94**, 1377 (1990).
[36] C. Xu, G. R. Burton, T. R. Taylor, and D. M. Neumark, J. Chem. Phys. **107**, 3428 (1997).
[37] R. E. Continetti, D. R. Cyr, R. B. Metz, and D. M. Neumark, Chem. Phys. Lett. **182**, 406 (1991).
[38] D. R. Cyr, R. E. Continetti, R. B. Metz, D. L. Osborn, and D. M. Neumark, J. Chem. Phys. **97**, 4937 (1992).
[39] GAUSSIAN 92, M. J. Frisch, G. W. Trucks, M. Head-Gordon, P. M. W. Gill, M. W. Wong, J. B. Foresman, B. G. Johnson, H. B. Schlegel, M. A. Robb, E. S. Replogel, R. Gomperts, J. L. Andres, K. Raghavachari, J. S. Binkley, C. Gonzalez, R. L. Martin, D. J. Fox, D. J. Defrees, J. Baker, J. J. P. Stewart, and J. A. Pople (Gaussian Inc., Pittsburgh, PA, 1992).
[40] J. T. Hougen, J. Chem. Phys. **36**, 1874 (1962).
[41] D. L. Osborn, D. H. Mordaunt, H. Choi, R. T. Bise, and D. M. Neumark, J. Chem. Phys. **106**, 10087 (1997).
[42] JANAF Thermochemical Tables, Vol. 14 (Supplement No. 1) (1985).
[43] R. D. Levine and R. B. Bernstein, *Molecular Reaction Dynamics and Chemical Reactivity* (Oxford University Press, New York, 1987).
[44] P. Pechukas and J. C. Light, J. Chem. Phys. **42**, 3281 (1965).
[45] P. Pechukas, J. C. Light, and C. Rankin, J. Chem. Phys. **44**, 794 (1966).
[46] M. Hunter, S. A. Reid, D. C. Robie, and H. Reisler, J. Chem. Phys. **99**, 1093 (1993).
[47] R. G. Gilbert, *Theory of Unimolecular and Recombination Reactions* (Blackwell Scientific Publications, Oxford, 1990).
[48] D. L. Osborn, H. Choi, D. H. Mordaunt, R. T. Bise, D. M. Neumark, and C. M. Rohlfing, J. Chem. Phys. **106**, 3049 (1997).